# SOIL AND FOUNDATION CONDITIONS RELATIVE TO EARTHQUAKE PROBLEMS

## ( SESSION I )

*The questions not answered in a written form by the author do not appear on the pages of discussion.*

# LATERAL EARTH PRESSURE AND STABILITY OF QUAY WALLS DURING EARTH-QUAKES

By HARUO MATUO[1] & SUKEO ŌHARA[2]

## PREFACE

After the great Kantô earthquake of 1923 in Japan, it became necessary to know the earth pressure which acts on the wall during earthquakes, in the reconstruction work of quay walls of Yokohama Harbour. Prof.Mononobe and Dr.Okabe proposed an idea to compute the pressure. They assumed that the resultant force due to max seismic acceleration and acceleration of gravity, acts statically, and adapting Coulomb's theory, computed the seismic earth pressure.

According to this computation, intensity of the earth pressure, to be added to static pressure, increases linearly as the depth.

But the experiment shows that this pressure is larger near the surface than near the bottom, contrary to the result above mentioned.

The authors here propose a new formula for it, and comparing with the results of their experiments, conclude that they bear good resemblance to each other.

Seismic hydraulic pressure and pore pressure of saturated earth were also observed in the experiment, and taking these values into account, the stability of typical quay walls of gravity type in Japan was calculated and the resistability against earthquakes of them is discussed.

## EARTH PRESSURE DURING VIBRATION

### a) Theoretical computation

Seismic earth pressure against a vertical wall was theoretically computed by assuming the earth as an uniform elastic mass of two dimensions. x axis is taken horizontally along the boundary surface at the base of a solid wall, and y axis vertically upward along the back surface of the wall (Fig 1a).

$$\left.\begin{aligned}(\lambda+\mu)\frac{\partial \Delta}{\partial x}+\mu\nabla^2 u+\rho k g \sin pt &= \rho\frac{\partial^2 u}{\partial t^2}\\ (\lambda+\mu)\frac{\partial \Delta}{\partial y}+\mu\nabla^2 u &= \rho\frac{\partial^2 u}{\partial t^2}\end{aligned}\right\} \quad \cdots\cdots (1)$$

Boundary conditions

$$i)\ (u)_{x=0} = (u)_{y=0} = 0$$

---

1 Professor, Kyûshû University, Fukuoka City, Japan.
2 Assistant Professor, Yamaguchi University, Ube City, Japan.

i) $(v)_{x=0} = (v)_{y=c} = 0$

ii) $(\lambda\Delta + 2\mu \frac{\partial v}{\partial y})_{y=H} = 0$

iii) $\mu(\frac{\partial u}{\partial y} + \frac{\partial v}{\partial x})_{y=H} = 0$

where $u$, $v$ = Components of displacements for x and y direction.

$\lambda$, $\mu$ = Lamé's elastic constants.

$k$ = Seismic coefficient.

$\rho$ = Density

General solution of the equation is not easy, but the solution for (1) has intermediate values between the two extreme cases of (A) and (B).

(A) When the displacement of y direction is perfectly restricted,

(B) When no resistance exists against the displacement of y direction.

For both these cases the following equation holds good

$$c_1^2 \frac{\partial^2 u}{\partial x^2} + c_2^2 \frac{\partial^2 u}{\partial y^2} + kg \sin pt = \frac{\partial^2 u}{\partial t^2} \qquad \cdots\cdots \quad (2)$$

Boundary conditions,

i) $(u)_{x=0} = (u)_{y=0} = 0$

ii) $(\frac{\partial u}{\partial y})_{y=H} = 0$

For the equation (2), the solution is easily obtained as follows

$$u = \frac{kg}{p^2}\left\{\frac{2}{H}\sum_m \frac{-\frac{2H}{2(m+1)\pi}\left(\frac{p}{c_2}\right)^2}{\left(\frac{(2m+1)\pi}{2H}\right)^2 - \left(\frac{p}{c_1}\right)^2} e^{-\frac{c_2}{c_1}\sqrt{\left(\frac{(2m+1)\pi}{2H}\right)^2 - \left(\frac{p}{c_2}\right)^2}\cdot x} \cdot \sin\frac{(2m+1)\pi}{2H} y \right.$$

$$\left. + \tan\frac{p}{c_2} H \cdot \sin\frac{p}{c_2} y + \cos\frac{p}{c_2} y \right\} \sin pt \qquad \cdots\cdots \quad (3)$$

and from this we have as the max half amplitude $\sigma_x$ of vibrating pressure at the wall as

$$(\sigma_x)_{x=0} = -\rho \sum_m \frac{4kg \sin pt}{\pi(2m+1)\sqrt{\frac{c_2^2}{c_1^2}\left(\frac{(2m+1)\pi}{2}\right)^2 - \left(\frac{pH}{c_1}\right)^2}} \cdot \sin\frac{(2m+1)\pi}{2} \cdot \eta \quad \cdots \quad (4)$$

in which $\eta = y/H$

Here for the case (A) $c_1^2 = \frac{\lambda+2\mu}{\rho}$, $c_2^2 = \frac{\mu}{\rho}$

and for the case (B) $c_1^2 = \frac{E}{\rho(1-\nu^2)}$, $c_2^2 = \frac{\mu}{\rho}$

$E$ = Young's Modulus; $\nu$ = Poission's ratio.

The value of $\sigma_x$ for (A) is larger than for (B); The difference between the two being about 10% when $\nu = 0.3$.

For safety's sake we may take the equation for the case (A) as the approximate equation of (1), and the solution of which as the approximate one for the design of aseismic quay walls.

Furthermore it was found by another research of ours that the values of $c_1^2$ and $c_2^2$ changes in proportion to the depth from the earth surface. Therefore equation (2) is changed to the equation having variable coefficients as follows,

$$\frac{\partial^2 U}{\partial t^2} = \frac{c_1^2}{a^2}(1-\alpha_1\eta)\frac{\partial^2 U}{\partial \xi^2} + \frac{\partial}{\partial \eta}\left[\frac{c_2^2}{H^2}(1-\alpha_2\eta)\frac{\partial U}{\partial \eta}\right] + \frac{kg}{H}\sin pt \qquad \ldots\ldots (5)$$

Boundary conditions

i) $(U)_{\xi=0} = (U)_{\eta=0} = (U)_{\xi=1} - 0$

ii) $\left(\frac{\partial U}{\partial \eta}\right)_{\eta=1} = 0$

where $\xi = \frac{x}{a}$, $\eta = \frac{z}{H}$, $U = \frac{u}{H}$

Ritz's approximate solution was applied and we have the approximate solution as follows.

$$U = \sum_{mn} A_{mn} \sin\frac{(2m+1)\pi}{2}\eta \cdot \sin(2n+1)\pi\xi \cdot \sin pt \qquad \ldots\ldots\ldots (6)$$

and from this $\sigma_x$ as follows;

$$(\sigma_x)_{x=0} = -c_1^2(1-\alpha_1\eta)\rho\frac{H}{a}\sum_{mn}(2n+1)\pi A_{mn}\sin\frac{(2m+1)\pi}{2}\eta\cdot\sin pt \ldots\ldots (7)$$

When there is surcharge of intensity q on the earth surface, The equation (5) is to be solved by the following boundary conditions.

i) $(U)_{\eta=0} = 0$

ii) $\frac{\rho c_2^2(1-\alpha_2)}{H}\left(\frac{\partial U}{\partial \eta}\right)_{\eta=1} = \frac{kq}{H} + p^2\frac{q}{g}(U)_{\eta=1}$

iii) $(U)_{\xi=0} = (U)_{\xi=1} = 0$

In this case as Ritz's solution cannot be applied, and therefore different method was applied and $\sigma_x$ was obtained.

b) Experiments

In the experiments which were carried out in our laboratory, the intensity of the horizontal earth pressure was measured at the end of a box on a shaking table.

Two kinds of end walls were used, "fixed" vertical wall and "movable" one, both perpendicular to the direction of vibration.

The shaking table(Fig 2) was supported by 4 vertical rigid steel strips with free hinged ends, and laterally supported by two pairs of spiral springs, and was driven by a crank shaft connected to an eccentric disc. Two kinds of boxes were used; the one a steel box having the dimensions 40(height) × 90(width) × 100(length), and the other a wooden box with a glass side 40 × 50 × 100cm.

Earth pressure was measured by pressure cells with a disk of 3.4cm diameter connected to a steel cross beam. The deformation of the beam was measured by electric strain meters attached to it. (Fig 3) The deformation of the beam at the center was $0.5 \times 10^{-4}$ mm/g/cm$^2$.

In the first experiment dry sand was carefully filled in the box and pressure changes were measured at 3 different heights along the centre line of the end wall.

The results in case of a "fixed" wall are shown in Fig 4 and 5a. The sand had mean diameter of 1.0mm and uniformity coefficient of 6.1; the period of vibration being $T = 0.3^{sec}$. After the dry sand was filled uniformly in loose condition, the vibration was given in such a way that the amplitude gradually increases for about 7 seconds, and then remains constant for about 10 seconds, and then

gradually decreases to a standstill in about 7 seconds. Fig 4 shows the double amplitude of pressure change at the beginning of vibration, and Fig 5a is the record of pressure during vibration.

As may be seen from Fig 4, the amplitude of pressure change is large at middle height, the phase of pressure change being the same throughout the whole depth. Fig 2a shows that there was no phase difference between the pressures of 3 different heights.

Fig 5b is the record of pressure in case of a "movable" wall. In this case a wall with a hinge at the lower end was vertically supported by a rod resting on an elastic spring plate. From this experiment we could see that

1) Max. amplitude of pressure decreases as the displacement increases, so long as the displacement is below a certain value.

2) When the amount of displacement exceeds the value, phase difference appears between the pressures at different heights, as shown in Fig 5b.

Two series of field experiments are now going on. Earth pressure acting on a concrete wall (Height 1.5m, width 0.9m, length 2.0m) is measured at 5 different heights (Fig 6). Vibration is given 1) externally by an oscillator of 1 HP. set at the distance of 4.5m from the wall surface, and 2) internally by the oscillator of 200 Watts set at the top of the wall. The acceleration and displacement are measured at 3 different heights on the wall. Some of the results are shown in Fig 7 and Fig 8. By comparing the results of externally and internally excited vibrations, actual seismic earth pressure may be computed. The results of which will be made public at the next chance.

c) Comparison of the theoretical and experimental results.

Elastic constants of the sand were determined by another experiments; and from these constants $G_1^2$ , $G_2^2$ , $\alpha_1$ and $\alpha_2$ were determined. Applying these values for the solution of equation (5), the seismic earth pressure for a "fixed" wall was computed and the results are shown in Fig 9. The distribution of pressure is akin to that of observed values (Fig 4).

In Fig 10 total amplitudes of pressure are plotted against k for 3 different heights. In this figure mean values can be roughly represented by the chain lines, excluding the values larger than $k = 0.3$ . At larger acceleration than $k = 0.3$, relative movement of sand particles occurs, which is not assumed in our computation.

In the figure the full lines, which indicate the computed values corresponding to the observed ones, are lower than the chain lines. But the inclinations of the two lines are nearly the same. This may be attributed to the effect of side walls of the box and the elasticity of the pressure cells.

Here, "total" amplitude does not always mean double amplitude; at small depth, static pressure becomes less than absolute value of the vibrating minus pressure when k exceeds a certain value, but as there is no tension between the earth mass and the wall, the "total" amplitude at such a depth is smaller than the double amplitude and equal to the sum of the static pressure and the half amplitude. As plus and minus pressures can not be distinguished in the observation, the total amplitudes of pressures are plotted and compared with the computed value.

An approximate solution for the movable wall was obtained by adding the solution of the following formula (8) to the solution of (5) of fixed wall (Fig 3b). This is the solution when the wall itself rotates by the angular amplitude $\beta$.

$$\frac{\partial^2 U}{\partial t^2} = \frac{C_1^2}{a^2}(1-\alpha_1\eta)\frac{\partial^2 U}{\partial \xi^2} + \frac{\partial}{\partial \eta}\left[\frac{C_1^2}{H^2}(1-\alpha_2\eta)\frac{\partial U}{\partial \eta}\right] \quad \cdots\cdots \quad (8)$$

Boundary conditions

i) $(U)_{\xi=0} = \beta\eta\sin pt$

ii) $(U)_{\xi=1} = (U)_{\eta=0} = 0$

iii) $\left(\frac{\partial U}{\partial \eta}\right)_{\eta=1} = 0$

To solve (8), put

$$U = \sum_{mn} A_{mn} \sin\frac{(2m+1)\pi}{2}\eta \cdot \frac{\sinh\sqrt{\lambda_n}(1-\xi)}{\sinh\sqrt{\lambda_n}} \sin pt \quad \cdots\cdots \quad (9)$$

where

$$U = \frac{u}{H}, \quad \xi = \frac{x}{a}, \quad \eta = \frac{y}{H}$$

Applying Ritz's approximate solution, $\lambda_n$ was determined, and then approximate values of $A_{mn}$. $(\sigma_x)_{x=0}$ should be determined from (9), but when x = 0, $\sigma_x$ does not converge,

$$(\sigma_x)_{x=\varepsilon} = C_1^2(1-\alpha_1\eta)\rho\sum_{mn}\frac{H}{a}\sqrt{\lambda_n}\cdot A_{mn}\sin\frac{(2m+1)}{2}\eta \times \frac{\cosh\sqrt{\lambda_n}(1-\varepsilon)}{\sinh\sqrt{\lambda_n}} \quad \cdots\cdots \quad (10)$$

was taken as the approximate value of $(\sigma_x)_{x=0}$, where $\varepsilon$ is infinite^simal value.

The solution of (8) has sign opposite to the solution of (5) and the resulting distribution of pressure becomes as shown with full line in Fig 11. From this, the phenomena that the pressure of different heights has opposite signs(Fig 11 and 5b) can be explained.

## PORE PRESSURE DURING VIBRATION

### a) Experiment

Next, we carried out experiments with sand saturated with water. Dry sand was pored into a steel box(40 × 90 × 100cm),partially filled with water, which was used in previous experiments and thus sand saturated with water waa obtained. One of the results of the experiments with saturated sand is shown in Fig 12b and is compared with a result of dry sand experiment (Fig 12b). In Fig 12a the amplitude of pressure may be said to be proportional to the acceleration, but in Fig 12b an extraordinary phenomenon of sudden increase of mean pressure occurs soon after the beginning of vibration.

By repetition of the experiment as shown in Fig 13 , it may concluded that:

(1) The sudden increase of mean pressure occurs at a definite acceleration and with a definite sand, in whatever mode the vibration may be given.

(2) This extraordinary phenomenon does not occur again so long as the vibration is under k = 0.5, and the phenomenon does not repeat itself unless the sand is newly refilled in the box. (Fig 13)
(3) Simultaneously with the phenomenon sand settles down rapidly (Fig 14), and water is squeezed out to the surface.
(4) When gravel is used for the back filling, this phenomenon does not occur. (Fig 13b)

To verify the ordinary pore pressure change due to vibration, experiments were made after the sand had fully settled down, viz. after the above phenomenon had occurred. Hydraulic pressure was measured by pressure cells with filters of brass plate having many holes 1mm in diametre. (Fig 3b) The results are shown in Fig 15 , where observed values have a tendency to increase in proportion to depth, but are greater than those values computed according to Westergaard's formula. For the sand, the discrepancy becomes greater also with the increase of the acceleration of vibration.

Discrepancy amounts to 40% of the computed values at its max. The reason of the discrepancy can not yet be fully explained, but for the present the surplus pressure may be due to the movement of sand particles caused by vibration.

b) Comments on the result of the experiment

Sudden increase of mean pore pressure is accompanied by the sudden increase of settlement when k = 0.2 ~ 0.25 (Fig 13), while the settlement of dry sand is nearly proportional to k. The sudden increase of pressure may be attributed to the sudden decrease of void caused by the relative movement of sand particles due to vibration. This pore pressure can not be released instantaneously from sand of low permeability, and caused liquifaction of sand. Thus the pore pressure at this moment is expected to be equal to the pressure of liquified sand.

Pressure increase for sand, computed according to the above assumption, nearly coincides with the observed value. (Fig 16) The above-mentioned explanation is justified by the facts that the pressure increase is smaller for gravel than for sand, and that it occurs only for loosely packed sand and never again after it had once occurred. For prototype quay walls, especially for those of gravity type, as rip-rup is usually used for back filling, this phenomenon is not expected to occur at the wall, and therefore the extraordinary increase of mean pressure is not taken into account in the stability calculation to be referred later.

As to the periodical pore pressure change, it was concluded by our theoretical solution that the following condition must be satisfied in order that the Westergaard's or Sundquist's pressure should be developed,

$$\left(\frac{\rho_w \lambda g p}{\pi \alpha}\right)^2 \ll \left[\left(\frac{\pi}{2h}\right)^2 + \left(\frac{\rho_w}{\pi}\right) p^2\right]$$

in which $\rho_w$ , Density of water; $\lambda$ , Porosity
$p$ , Angular velocity of vibration
$h$ , Depth of water
$\pi$ , Bulk Modulus of water
$\alpha$ , Permeability of the earth

For the stability calculation of the prototype quay walls, the

pore pressure change was computed according to Sundquist's formula, viz. the modified Westrgaard's formula, assuming that the width of the rip-rup is the same as the height of the wall, and further back it is reclaimed with silty sand of relatively small permeability. In this case the pore pressure change is calculated to be 70% of Westergaard's value.

For smaller permeability than $\alpha = 10^{-1} \sim 10^{-3}$ cm/sec corresponding the period of vibration T = 0.3 ~1.0 sec, it was shown by that solution that above pressure change due to vibration is pretty small.

## RESISTABILITY OF QUAY WALLS AGAINST EARTHQUAKES

### a) Earth pressure diagrams

Max earth pressure against quay walls during earthquakes is calculated according to formula (7), assuming the wall to be "fixed", and it is shown in Fig 17. In the calculation of stability, total earth pressure is obtained by adding above pressure to ordinary static earth pressure. Here $\rho$ is taken as 1.6gr/cm$^3$, and the elastic constants of the back filling is taken as shown in the accompanying figure in Fig 17. Total pressure $P = k\psi$, where k is the seismic coefficient, and $\psi$ is to be read on the diagram for various surcharge $q$. The height of point of application of the resultant pressure can be read on the upper diagram. Here the resonance of the earthquake vibration and earth pressure is disregarded, assuming the period of earthquake vibration is pretty larger than that of earth pressure period.

To make the calculation simple, the width of the whole back-filling was assumed 10 times as large as the quay wall height, because the seismic pressure thus calculated is approximately the same with infinitely long back-filling. When seismic earth pressure and pore pressure are at their max, the water pressure to the wall from the sea decreases in accordance to the Westergaard's formula, and it is under this condition that the stability of the wall is calculated.

### b) Resistability of quay walls against earthquakes

By 4 great earthquakes of Kantô(1923), Sizuoka(1935), Nankai(1946), and Tokachi(1952), 23 gravity type quay walls underwent damages, in which 16 were sliding at the base, and 7 were sliding and overturning combined (Fig 19). From this it may be said that prodominant failure is sliding. Thus the resistability of existing typical quay walls in Japan against sliding was calculated under the assumption that the seismic earth pressure acts against "fixed" walls, and that the above-mentioned hydraulic and pore pressures act to the walls.

The effect of yielding of wall on seismic earth pressure is neglected, and it was also assumed that no resonance occurs between the ground motion and seismic earth pressure.

The calculation was made for the following cases.

$$\frac{h}{H} = 0.7 \sim 0.9 \text{ (Fig 18)}, \qquad \frac{B}{H} = 0.6 \sim 0.8$$

Most existing quay walls of gravity type are included in these ranges. Unit weight of wall material $\rho = 2.0$gr/cm$^3$. Fig 18 shows the critical seismic co-efficient for various values of $\frac{h}{H}$ and $\frac{B}{H}$ for various heights when there is no surcharge on the

earth surface. (q = 0) From this it may be said that the max. seismic coefficient which ordinary gravity type quay walls can resist is $k_c = 0.1 \sim 0.12$. On the other hand, damages of gravity type quay walls hitherto had occurred in the region of seismic scale V or over according to Japanese Meteological Observatory.

The acceleration of the earthquake of scale V is roughly estimated as $k_c = 0.10 \sim 0.25$. It is a fact of some interest that the lower limit nearly corresponds to the above-mensioned values of $k_c$, which is the limit of the quay walls' resistance against sliding.

## CONCLUSIONS

According to theoretical study, the distribution of seismic earth pressure is computed as shown in Fig 9, and total pressure and point of application acting on a vertical wall were calculated as shown in Fig 17. For this calculation it was assumed that the wall is "fixed", not allowing any relative displacement against the ground, and that there is no resonance between the ground motion and the earth pressure. These conditions may not be satisfied always, and for the case further research is expected in future. The results of experiments may be said nearly to coincide with the theoretical computation for "fixed" wall.

Theoretical computation for "movable" wall could explain the experimental fact that the seismic pressures of plus and minus values coexist at different heights of the wall. The phenomenon of liquifaction of saturated sand due to vibration was observed, but it was concluded that, when there is rip-rup between the wall and the sand-filling, the pressure of liquefied earth does not act on the wall.

It was also shown that the max pore-pressure-increase during earthquakes is approximately equal to Westergaard's hydrodynamic pressure, and that for stability calculation of quay walls of ordinary gravity type in Japan, 70% of that value should be adapted.

The water pressure on sea side decreases when horizontal acceleration of earthquake is in the direction of land-side, viz when the seismic earth pressure and pore pressure are at their max.

By those assumptions, the resistability of typical gravity type quay walls by 4 great recent earthquakes in Japna may be said to coincide with the result of our study.

## ACKNOWLEDGEMENT

The authors wishes to express their sincerest thanks to Messrs. Mituhisa Kajiwara of Japan Highway Corporation, Hirosi Matuo of KyûshûUniversity, and members of Hakata Harbour Construction Office of Ministry of Transportation, for their cooperation on our experiment.

## BIBLIOGRAPHY

Mononobe, N. "Design of aseismic Gravity Wall"
Report of Kantô Earthquake Damages of 1923. J.S.C.E. Vol 3, 1925.

Okabe, S. "General Theory of Earth Pressure and Seismic Stability of Retaining Wall and Dam."(in English) Jour. J.S.C.E. Vol 12, No. 1, 1924.

Mononobe, N. & Matuo, H. "Experimental Investigation of Lateral Earth Pressure during Earthquakes."(in English). Bull.Earthquake Research Inst. Tokyo Univ. Vol.X Part 4. 1932.

Mononobe, N. & Matuo, H. "On the determination of Earth Pressure during Earthquakes." (in English) World Engineering Congress, Tokyo 1929. Paper No. 388.

Matuo, H. "Damages to the Quay Walls of Simizu Harbour." (in English) Bull. Earthquake Research Inst. Tokyo Univ. Vol XIII part 4, 1935.

Matuo, H. "Experimental Study on the Distribution of Lateral Earth Pressure in Earthquakes." Jour. J.S.C.E. Vol.27, No.2, 1941.

Matuo, H. & Ohara, S. "Seismic Earth Pressure due to Saturated Soils " Jour. J.S.C.E. Vol 40, No.6, 1955.

Matuo, H. & Ohara, S. "Dynamic Pore Pressure acting to Quay Walls during Earthquakes." Transactions, J.S.C.E. No. 38, 1956.

Matuo, H & Ohara, S. "Seismic Earth Pressure against Quay Walls." Technical Report of Kyushu Univ. Vol.29, No 2, 1956; Vol 30, No.1, 1957; Vol 31, no.2, 1958.

Ohara, S. "Dertermination of Elastic Constants of Sand" Transactions, J.S.C.E. No.38,1956.

Kajiwara, M. "Oscillatory Characteristics of Rigid Body on Elastic Foundation " Transactions, J.S.C.E. No 55, 1958.

Ichikawa, M. & Niwa, S. "Experimental Studies of Seismic Earth Pressures." Report No.1 and No.2 , Transactions, J.S.C.E. No.38 and No 39 , 1956.

Niwa, S. "Study on Vibrating Earth Pressure." Monthly Reports of Transportation Technical Ressearch Institute,Vol. 8, No.3, 1958.

Westergaard, H.M. "Water pressures on Dams during Earthquakes." Trans. A.S.C.E. Vol 98,1933.

Tschbotarioff, G.P. "Soil Mechanics, Foundation and Earth Structures" McGraw Hill Co. 1952.

## NOMENCLATURE

$a$ = Length of the earth filling

$c_1^2 = \frac{\lambda+2\mu}{\rho}$ or $\frac{E}{\rho(1-\nu^2)}$

$c_2^2 = \frac{\mu}{\rho}$

$E$ = Young's modulus

$k$ = Seismic co-efficient viz. acceleration of earthquake divided by acceleration of gravity

$k_c$ = Critical seismic co-efficient of wall failure

$H$ = Height of the wall

$h$ = Depth of water before the wall

$p = \frac{2\pi}{T}$

$T$ = Period of vibration

$\eta = \frac{y}{H}$

$u$ = Horizontal displacement

$v$ = Vertical displacement

$\alpha$ = Permeability of earth

$\alpha_1$ = Variation co-efficient of $c_1^2$ due to depth from the earth surface.

$\alpha_2$ = Variation co-efficient of $c_2^2$ due to depth from the earth surface

$\beta$ = Angular displacement

$\Delta = \frac{\partial u}{\partial x} + \frac{\partial v}{\partial y}$

$\eta = \frac{y}{H}$

$\kappa$ = Bulk modulus of water

$\lambda$ = Lame's elastic constant; or Porosity of the earth

$\mu$ = Lame's elastic constant

$\nu$ = Poisson's ratio

$\xi = \frac{x}{a}$

$\rho$ = Density of the earth

$\rho_w$ = Density of water

$\psi$ = Seismic earth pressure co-efficient

$\nabla^2 = \frac{\partial^2}{\partial x^2} + \frac{\partial^2}{\partial y^2}$

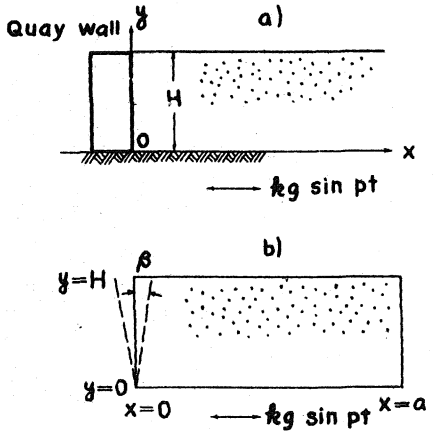


Fig. 1 a) Fixed Wall
b) Movable Wall

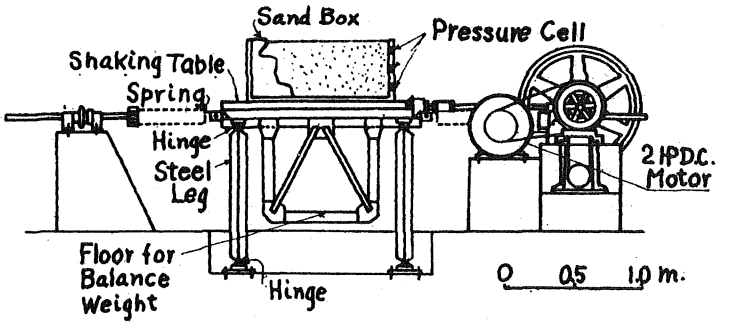


Fig. 2 Shaking table

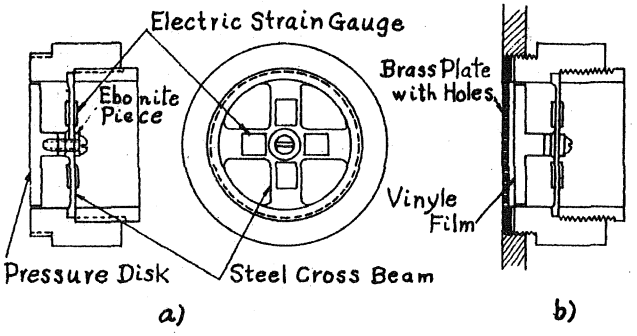


Fig. 3 Pressure cells
a) for earth and pore pressure,
b) for pore pressure only.

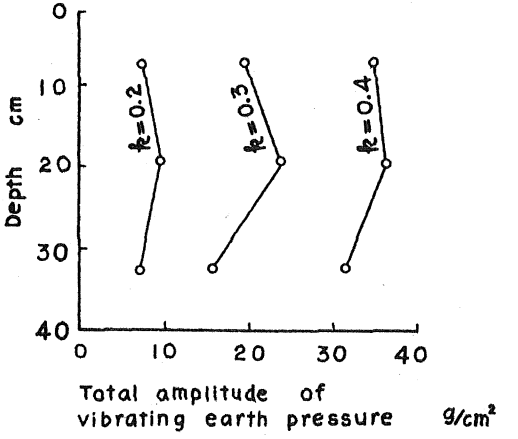


Fig. 4 Amplitude of vibrating pressure for rigid wall at 3 different heights (observed mean values).

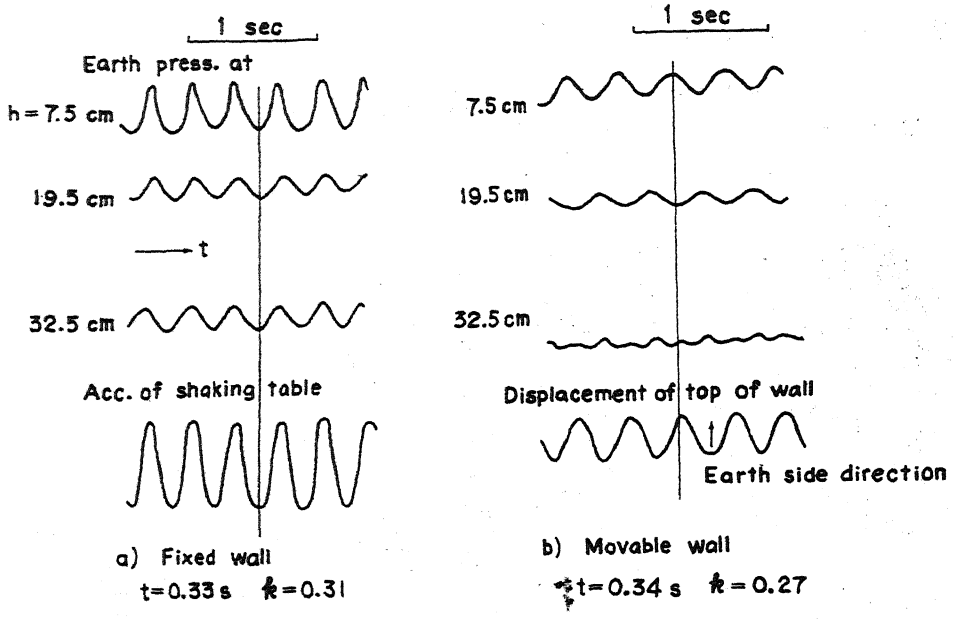


Fig. 5 Record of pressure change at 3 different heights as compared with the acc. of the shaking table or the displacement of the top of the wall.
a) Fixed wall - for 3 heights the phase is the same.
b) Movable wall - here the phase of 7.5 cm is different from 19.5cm.

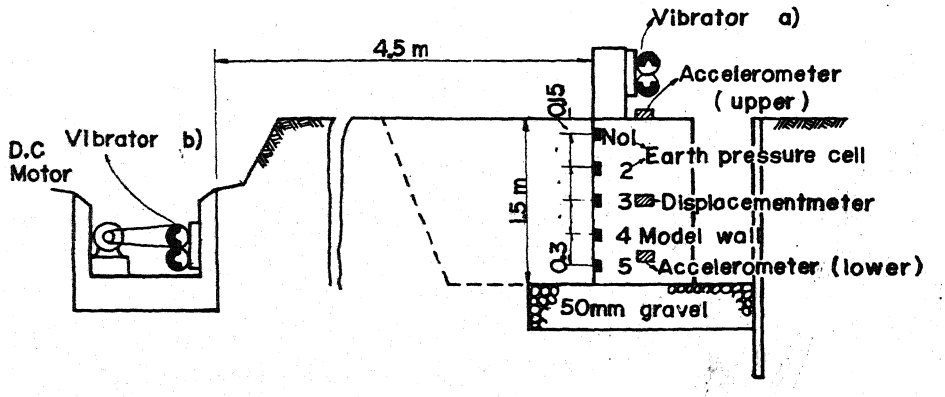


Fig. 6 Field test arrangements.

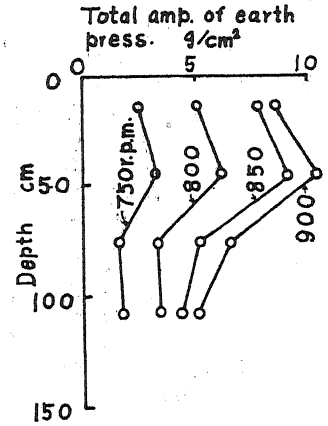


Fig. 7 Field test results, when vibration was given to the ground at 4.5m distant from the wall.

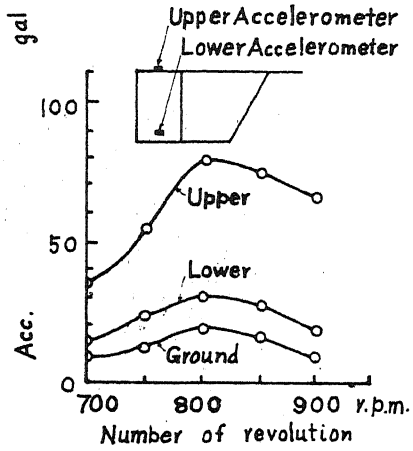


Fig. 8 Field test results, when vibration was given to the ground at 4.5m distant from the wall.

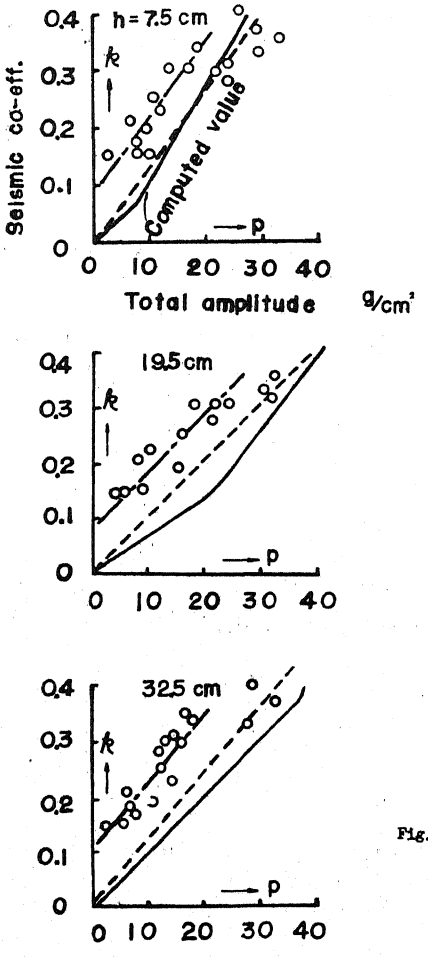


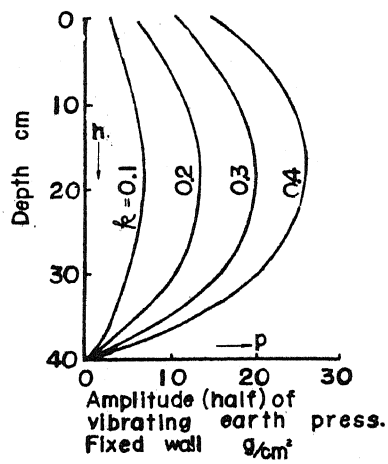


Fig. 9 Computed amplitude of vibrating earth pressure (half amp.); fixed wall.

Fig. 10 Observed and computed value at 3 different heights. Full line is computed values, and the chain line is the mean observed value.

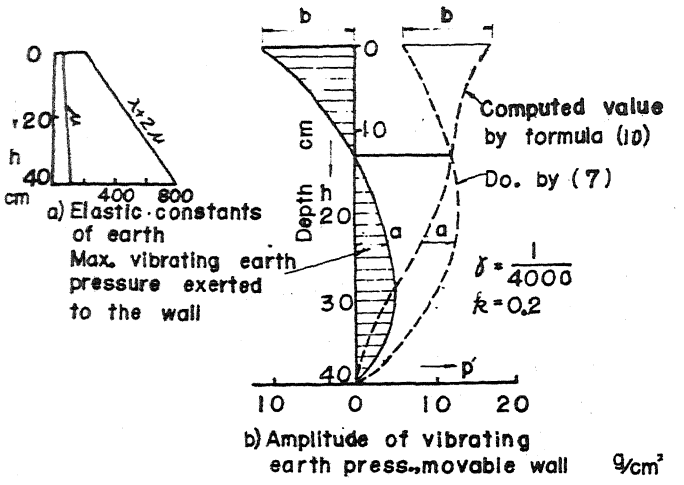


Fig. 11 Computed pressure to be exerted to a movable wall.

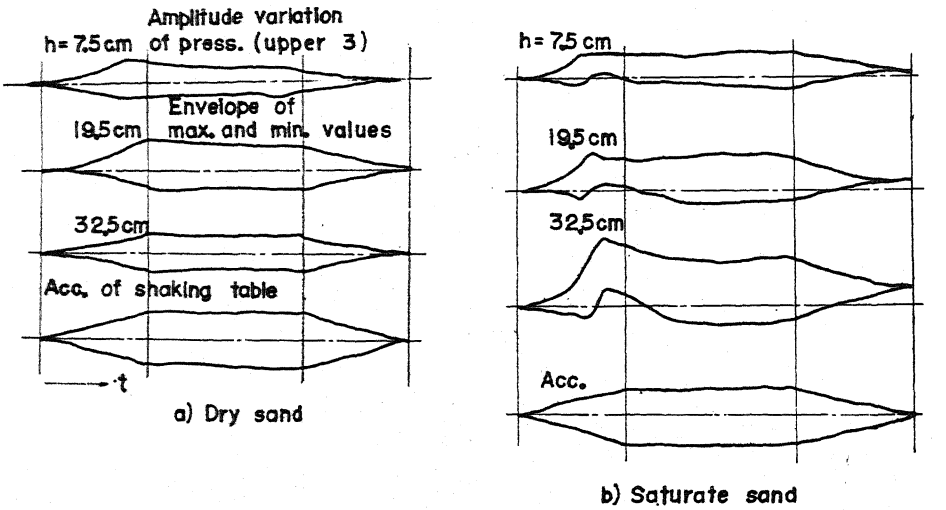


Fig. 12 Pressure variations when vibration was given as shown in the lowest figures; envelopes of max and min values are shown.

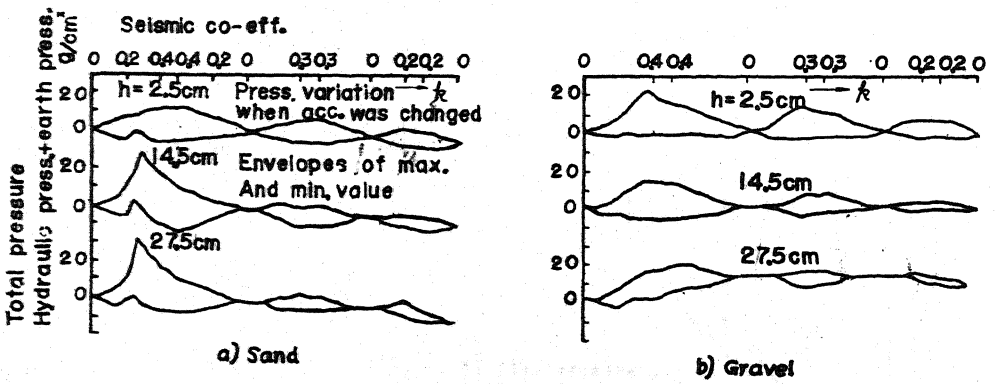


Fig. 13 Pressure variations at 3 different heights, when the vibration of seismic coefficient k was given as shown at the top. Pressure variations are shown by envelopes of max and min values. Acceleration was gradually increased and decreased. Everytime the max k is changed as shown in the figure, a) sand b) gravel.

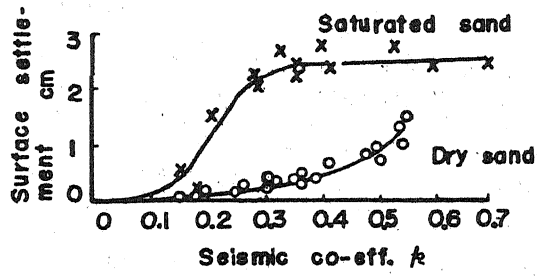


Fig. 14 Surface settlement versus acceleration.

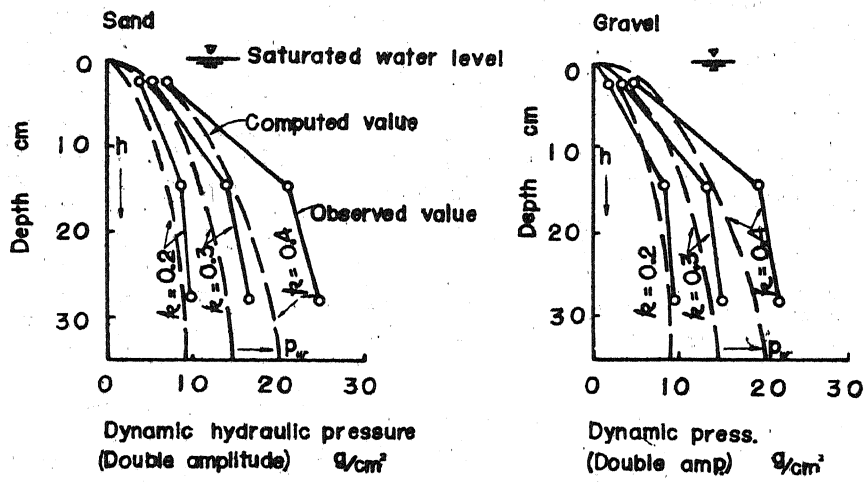


Fig. 15 Dynamic hydraulic pressures of sand and gravel, as observed and computed.

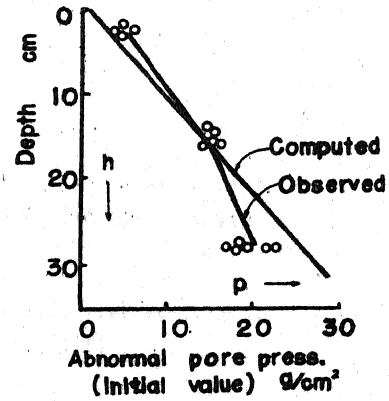


Fig. 16 Abnormal pore pressure which occurs at the beginning of vibration, observed and computed values.

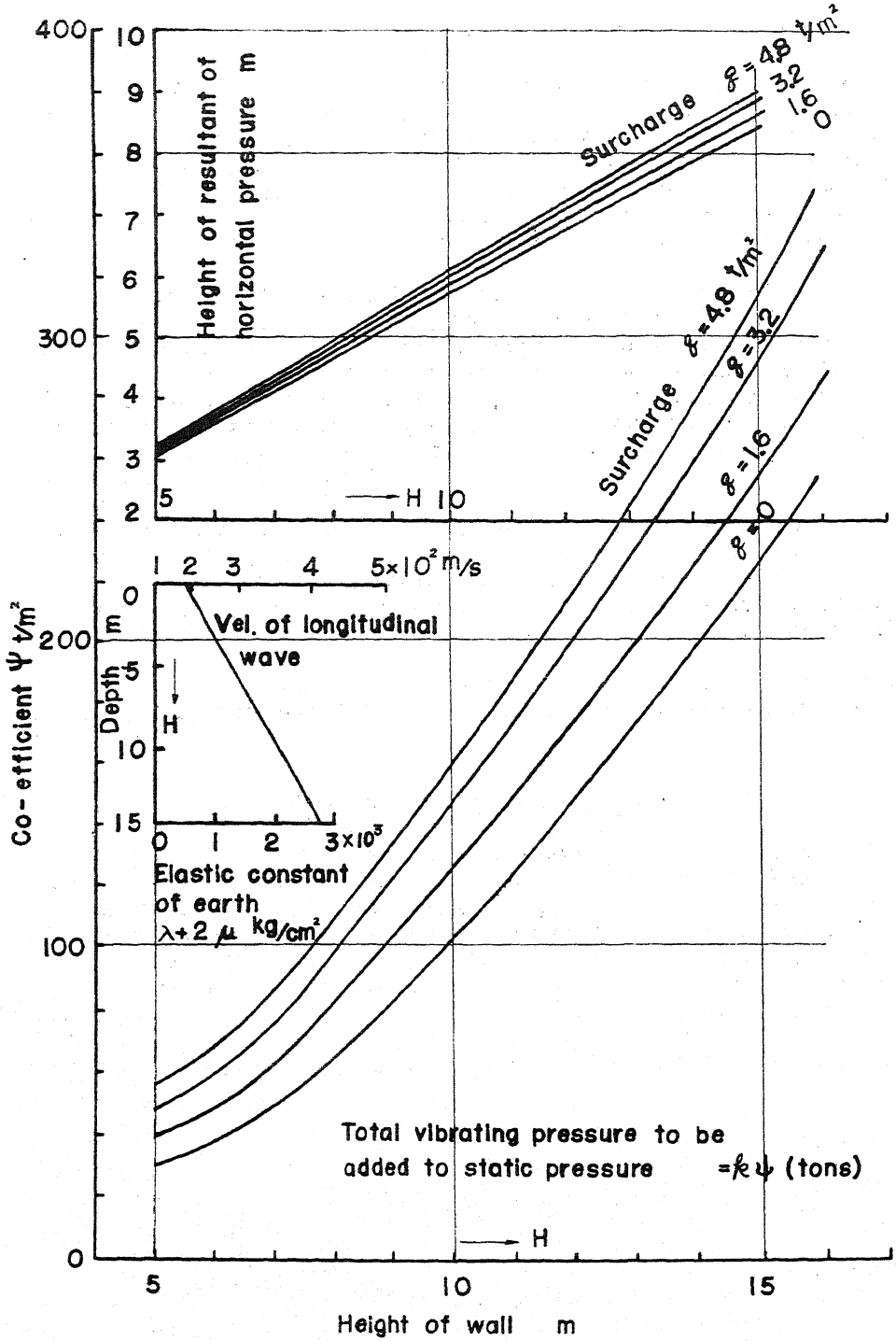


Fig. 17 Computed earth pressures which should be added to static pressures and point of application of the resultant force.

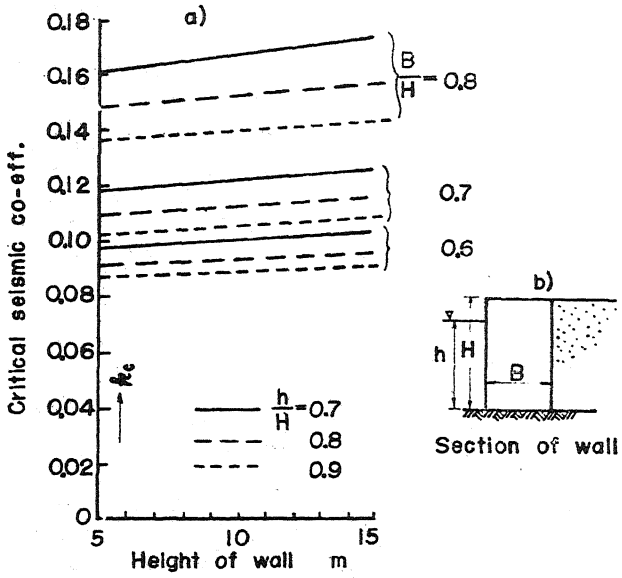


Fig. 18 Resistability of typical concrete quay walls against earthquakes.

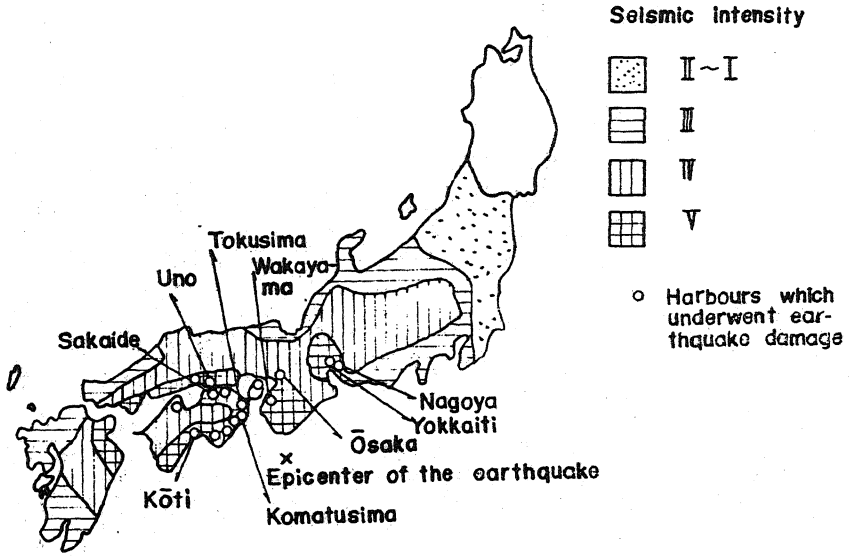


Fig. 19 Seismic Intensity of Nankaidô Earthquakes in 1946, and the site of harbour in which quay walls underwent severe damages.